This article was published in FEBS Journal, 282(12), 2309-2316, 2015
http://dx.doi.org/10.1111/febs.13275

Enzyme kinetics: the whole picture reveals hidden meanings

Maria F. Pinto[1], Berta N. Estevinho[2], Rosa Crespo[1], Fernando A. Rocha[2], Ana M. Damas[1] and Pedro M. Martins[1,2]

[1] Instituto de Ciências Biomédicas Abel Salazar (ICBAS), Universidade do Porto, Portugal

[2] Laboratório de Engenharia de Processos, Ambiente, Biotecnologia e Energia (LEPABE), Departamento de Engenharia Química, Faculdade de Engenharia da Universidade do Porto, Portugal

The methodology adopted by Michaelis and Menten in 1913 is still routinely used to characterize the catalytic power and selectivity of enzymes. These kinetic measurements must be performed soon after the purified enzyme is mixed with a large excess of substrate. Other time scales and solution compositions are no less physiologically relevant, but fall outside the range of applicability of the classical formalism. Here we show that the complete picture of an enzyme's mode of function is critically obscured by the limited scope of conventional kinetic analysis, even in the simplest case of a single active site without inhibition. This picture is now unveiled in a mathematically closed form that remains valid over the reaction time for all combinations of enzyme/substrate concentrations and rate constants. Algebraic simplicity is maintained in the new formalism when stationary reaction phases are considered. By achieving this century-old objective, the otherwise hidden role of the reversible binding step is revealed and atypical kinetic profiles are explained. Most singular kinetic behaviors are identified in a critical region of conditions that coincide with typical cell conditions. Because it is not covered by the Michaelis–Menten model, the critical region has been missed until now by low- and high-throughput screenings of new drugs. New possibilities are therefore raised for novel and once- promising inhibitors to therapeutically target enzymes.

Introduction

One hundred years since it was first proposed, the Michaelis–Menten (MM) equation [1,2] has received renewed interest in areas such as drug discovery [3,4], systems biology [5–7] and single-molecule enzymology [8–10]. Despite the controversy about who else should be credited with its authorship [11], this formalism is today recognized as the steady-state approximation of the mechanism proposed 12 years later by Briggs and Haldane, comprising reversible formation of an enzyme–substrate complex (binding step) followed by its irreversible transformation into product and free enzyme (catalytic step) [8,12]. In a recognizable form of the MM equation, the hyperbolic dependence of the initial reaction rate v_0 on the initial substrate concentration S_0 is given as:

$$v_0 = \frac{v_{max} S_0}{S_0 + K_M} \qquad (1)$$

where v_{max} is the limit reaction rate for a given enzyme concentration $E0$, and K_M is the Michaelis constant. The rate constants associated with the reversible binding step ($k1$ and $k-1$) and the catalytic step ($k2$) are condensed in the two MM parameters as $v_{max} = k2\ E0$ and $K_M = (k-1 + k2)/k1$. The simplifying hypotheses required to derive Eqn 1 confine its applicability to the initial phases of reactions that start with enzyme concentrations much lower than the sum ($S0 + K_M$) [13–15]. However, as kinetic experiments should include $S0$ values well below K_M, the practical rule is that $S0 >> E0$ for the MM equation to hold true. If this region of validity is considered the 'white' region, it is as if we are ignoring the 'gray' and 'dark' zones of conditions for which $S0 \sim E0$ and $S0 \ll E0$, respectively. Expanding the analogy to reaction time scales other than the initial phases, it is as if we are ignoring a whole palette of gradations in our picture. This was necessary in order to render manageable a problem that in its simplest form involves three rate constants and four species changing over time [13,15–19]. Even so, one of the merits of the classical formalism is to summarize the influence of initial conditions ($S0$ and $E0$) on a pivotal variable ($v0$) that is easily measured by the accumulation of product over time given by a progress curve. By selecting the equally accessible pivotal variable $(S0 - P)/v$, in which $(S0 - P)$ is the con- centration of product still to be formed, and v is the instant reaction rate, we provide the complete portrayal of enzyme kinetics in a mathematically closed form.

Results and Discussion

Although the system of first-order differential equations describing the Briggs and Haldane mechanism does not have a known analytical solution, it becomes solvable after introducing the pivotal variable $(S0 - P)/v$. Derived in Doc. S1, the final solution is given in Experimental procedures by Eqn 4, and plotted in normalized units in Fig. 1A. The adopted simplifying hypotheses do not confine the validity of the new model to any limited conditions whatsoever (see discussion of approximations 1 and 2 in Doc. S1, and Figs S1 and S2). In the following form

$$\frac{S_0 - P}{v} = \tau[1 + \omega(s_0 \exp(s_0 - t/\tau))]\phi_C \qquad (2)$$

the pivotal variable is defined in terms of the Lambert ω function [14,20], whose argument includes the time dimension t and MM parameters incorporated in $s0 = S0/K_M$ and $\tau = K_M/v_{max}$. The expression ΦC is a time- dependent correction factor to account for the 'gray' and 'dark' regions. Its full definition is given by Eqn S23 (Doc. S1) as a function of $s0$, t/τ, $e0 = E0/K_M$ and the enzyme–substrate dissociation constant $K_S = k-1/k1$ (a non-MM parameter). In Fig. 1A, the model equation is normalized by $e0\tau$ ($=k\bar{2}^{1}$), while in Fig. 1B, only the definition of $\Phi C(t)$ is plotted.

Before discussing novel kinetic aspects that are beyond the MM border, we discuss those

that may be misleading within the MM border. In particular, we show how to avoid deceptive $v0(S0)$ profiles that result from disregarding the various time scales of product accumulation. This is illustrated for hydrolysis of the fluorogenic substrate 4−methylumbelliferyl-galactoside (MUG) by the enzyme β−galactosidase.

In our kinetic measurements, the enzyme was mixed with a large excess of MUG so that the MM conditions are respected. In the 'white' region of conditions ($s0 >> e0$), no 'gray'/'dark' corrections are required in Eqn 2 (Φ_C is approximately 1 in Fig. 1B). During the initial moments of the reaction, Eqn 2 is further simplified to the Hanes−Woolf linearization of the MM equation, $S0/v0 = \tau (1 + s0)$, provided that it may be assumed that t/τ is approximately 0 (and $P0 = 0$). In practice, however, reactions start to be effectively monitored after elapsed the lag time ($t$lag) comprising the time required to mix the solutions, the dead time of the instrument, and the period over which reaction rates are measured. For higher enzyme concentrations, $t\text{lag}/\tau$ overtakes the value of $s0$, and the equivalence between Eqn 2 and the Hanes−Woolf equation is lost. Figure 2A illustrates how the linearity is broken as the concentration of β−galactosidase increases from 0.052 μg-mL^{-1} (top panel) to 5.236 μg-mL^{-1} (bottom panel) (see also Fig. S3B). The supposedly hyperbolic vi ($S0$) relationship is confirmed for lower $E0$ (Fig. 2B, top panel) but becomes increasingly sigmoidal as $E0$ and $t$lag increase (Fig. 2B, bottom panel, and Fig. S3A), wrongly suggesting allosteric regulation properties similar to those that are characteristic of cytochrome P450, for example [4,21].

The reason why the MM equation cannot be applied is that, by missing the first moments of the reactions, we also miss the period of constant rate, particularly under conditions of low $S0$ and high $E0$. In such cases, the measured initial rates vi are lower than the true initial rate $v0$. A possible solution to this problem would be to adopt rapid-reaction set-ups [22,23]. Other alter- natives that do not require experimental reconfiguration include (a) progress curve fitting, and (b) Eqn 2 fitting. However, both non-linear regressions should be adopted parsimoniously; in the first case, the numerical fit is easily biased towards one of the constants $v$max or s, depending of the substrate concentration under investigation [24]. In the case of Eqn 2, the numerical fit is greatly affected by uncertainties associated with estimation of $t$lag preceding each measurement. Instead, we propose a straightforward alternative based on an additional simplification of Eqn 2 under conditions of $s0 >> e0$: in that region alone, the ($S0 - P$) term and the Lambert x term correspond to the direct and normalized definitions of the instant substrate concentration (S and s, respectively), thus reducing Eqn 2 to a Hanes−Woolf linearization relating S/v and S. Subtle as it may seem, using measured substrate concentrations instead of initial concentrations is sufficient to recover the linearity of the modified Hanes−Woolf plot (Fig. 2A, bottom panel) and the hyperbolic relationship (Fig. 2B, bottom panel). As shown in Fig. 2C,D, the new formalism produced estimates of $v$max and KM that were within the experimental error even for concentrations of b−galactosidase as high as 10.471 μg-mL^{-1}, the limit above which product accumulation for $t > t$lag is hardly discernible.

Only a slight modification to the MM equation is therefore required to account for the time dimension under the 'white' region of conditions, but what about the 'gray' and 'dark' regions involving $s0$ values around and below $e0$? This is where the dissociation constant

of the enzyme–substrate complex (K_S) may play its hitherto obscured role. As indicated by the solid and dashed lines in Fig. 1A,B and Fig. S4, the major differences between extremely low and extremely high substrate affinities are principally confined to enzyme concentrations around K_M (e_0 of approximately 1), here called the critical region of conditions, and to the early reaction phases when the enzyme is in excess over substrate ($e_0 > s_0$). Under these conditions, affinity-based mechanisms of enzyme regulation may be anticipated that do not necessarily involve inactivated enzyme–inhibitor complexes; these are not considered here. In the search for a universal, algebraically simple formalism [5,18,25], we chose the stationary instant t^* at which the pivotal variable $(S_0 - P^*)/v^*$ is independent of K_S (as demonstrated during derivation of Eqns S19 and S24 in Doc. S1):

$$\frac{S_0 - P^*}{v^*} = \frac{\tau}{2}(2 + s_0 + e_0 + |s_0 - e_0|) \qquad (3)$$

The additional simplifying hypothesis required to derive this equation does not compromise its applicability even in the worst-case scenario discussed in Doc. S1 for approximation 3. Because the stationary instant corresponds to the moment of highest reaction rate, it is unmistakably present in a full progress curve, and is not subject to the ambiguities of instantaneous reaction rate methods such as low signal-to-noise ratios. As shown below, the highest reaction rates may differ from initial reaction rates under non-MM conditions. Equation 3, the stationary version of the more generic model equation, may be used to estimate MM parameters by trivial linear regressions and without major experimental constraints other than the instrumental resolution required to access the stationary moments [22,26]. As an example, we studied the hydrolysis of the fluorogenic substrate 4–methylumbelliferyl-b–D-*N*, *N*',*N*''-triacetylchitotrioside (MUF-triNAG) by hen egg-white lysozyme (EWL). Substrate concentrations above and below the enzyme concentration were adopted in order to understand the peculiar 'gray'/ 'dark' regions (Figs S4 and S5). When substrate concentrations lower than E_0 are adopted, the reaction rates are advantageously measured at various enzyme concentrations and fixed S_0. As illustrated in Fig. 3A, in addition to being strongly affected by E_0, the pivotal variable is linearly dependent on E_0^{-1}, in conformity with Eqn 3 (note that s is alternatively defined as $\tau = K_M/k_2E_0$). In contrast, the stationary-state Hanes–Woolf plots (Fig. 3B) show a relatively weaker influence of S_0 at fixed enzyme concentrations. The reasons are twofold. First, and as suggested by Eqn 3, the pivotal variable $(S_0 - P^*)/v^*$ is independent of the substrate concentration for $S_0 < E_0$. Second, the span of substrate concentrations above E_0 was too small to have pronounced effects for $S_0 > E_0$. A single linear fit in Fig. 3A was sufficient to produce valid estimations over critical and transient conditions such as those in Fig. 3B (solid lines). This confirms that Eqn 3 is an adequate representation of the stationary pivotal variable, subject to diptych linear influences of (a) E_0^{-1} for $S_0 \approx E_0$ conditions (and fixed S_0), and (b) S_0 for $S_0 > E_0$ conditions (and fixed E_0).

While the problem of simple and universal estimation of MM parameters is solved, we have still ignored how to estimate the dissociation constant K_S. In fact, K_S is indirectly present in Eqn 3 as it determines the reaction rate and product concentration under

stationary conditions. If the scaled dissociation constant reaches its maximal value ($K_S/K_M = 1$), then $v^* = v_0$ and $P^* = 0$, thus reducing Eqn 3 to a MM- like equation for $S_0 > E_0$, and to the simplified Bajzer and Strehler equation [17] for $S_0 < E_0$. In all other cases, product accumulation curves are expected to show an inflection point at an instant $t^* > 0$ that becomes more noticeable for lower concentrations of enzyme and substrate (Fig. S6). Under K_S-sensitive conditions (e_0 and $s_0 \leq 1$), clearly hyperbolic progress curves (Fig. 3C, top panel) or invariant pivotal variable values during the initial reaction phases (Fig. 3C, bottom panel, and Fig. S4) immediately suggest that $K_S = K_M$ (11.1 μM), which compares well with literature K_S values between 5 and 33 μM obtained for the non-fluorogenic lysozyme−tri- NAG complex using advanced mass-spectrometry techniques [27]. If the progress curves were scenario, the value of K_S could be calculated from Eqn S26 in Doc. S1 using the $(S_0 - P)/v$ values measured after long reaction times. The usefulness of this kind of late-stage analysis may also be extended to single-assay estimations of the time constant τ in cases where the enzyme concentration is very low ($e \ll 1$) or unknown, such as in cell extracts (Fig. S5).

Besides triggering most singular kinetic behaviors, the critical region of concentrations around the K_M value is also biologically important for both enzyme and substrate [20,28−31]. Additionally, it is recommended that high-throughput screenings of lead compounds adopt substrate concentrations around or below K_M for optimal sensitivity to competitive inhibitors [32,33]. Whilst the chiaroscuro of an enzyme's clockwork is revealed by Eqn 2 (which is equivalent, in its extended form, to Eqn 4), we expect that Eqn 3 will help researchers unveil regulation mechanisms that remain hidden by the steady-state constraints. The critical region of conditions is here suggested as a favourable pathway to therapeutically target enzymes, and may justify taking rejected inhibitors back from the laboratory shelf.

In conclusion, in addition to filling all the major gaps left by the steady-state approximation, the present work opens new perspectives and opportunities for future kinetic studies in enzymology. First, a complete picture of non-inhibited, single active-site enzyme kinetics is unveiled for the first time in a mathematically closed form that is valid over all experimental conditions and not only conditions of great substrate excess (Eqns 2 or 4, and Fig. 1). Second, the new theoretical model is also valid over all reaction time scales, not only during the initial phases. Third, non-linear Hanes−Woolf plots (Fig. 2A, red, and Fig. S3B) or non-hyperbolic MM relationships (Fig. 2B, red, and Fig. S3A) may solely represent the inability of the MM equation to describe later reaction phases, even for conditions of great substrate excess. A method is proposed to promptly overcome this limitation (Fig. 2A,B, blue). Fourth, algebraic simplicity, a key aspect for the success of the MM equation, is maintained by the new formalism when stationary instants are considered (Eqn 3). This allows for simple and condition-independent determination of kinetic parameters. Fifth, the hitherto obscure role of the dissociation constant K_S is revealed (Fig. 1A,B and Fig. S4), thus completing the puzzle originally set by the Briggs and Haldane mechanism. When the initial enzyme concentration is around K_M, the dissociation constant influences all reaction phases; when the initial enzyme concentration is in excess over substrate, only early reaction phases are affected; under conditions of substrate excess, the K_S constant has no visible effect on the progress curves (in accordance with the MM equation). Six, two methods are proposed to estimate the value of K_S when initial (Fig. 3C) or later stages (Fig. S5 and

Eqn S26, Doc. S1) are analyzed. Seven, the most singular kinetic behaviors are found to take place in a critical region of conditions where the con- centration of enzyme and substrate are both close to K_M (Fig. 1A,B and Figs S4 and S5). It is not totally surprising that these conditions coincide with those usually considered as representative of the cell. Finally, the preceding conclusion, together with the possibility raised by the fourth conclusion, give support to a gradual change in compound libraries screening towards equimolar enzyme–substrate assays. By systematically adopting conditions of substrate excess, it is conceivable that *in vitro* drug discovery research has failed to identify therapeutically relevant inhibition/ regulation effects.

Experimental procedures

Reagents

Enzymes β–galactosidase from *Escherichia coli* and egg- white lysozyme (EWL) were obtained from Merck (Darmstadt, Germany) and used without further purification. The fluorogenic substrates 4–methylumbelliferyl-galactoside (MUG) and 4–methylumbelliferyl-b–D-*N*,*N*',*N*''-triacetylchi- totrioside (MUF-triNAG) were purchased from Sigma- Aldrich (Sintra, Portugal) and Carbosynth (Berkshire, UK), respectively. 2–mercaptoethanol was purchased from Sigma-Aldrich. All water used was double-distilled.

β–galactosidase enzymatic assay

Time progress curves were measured during hydrolysis of the non-fluorescent substrate MUG to the fluorescent product 4–methylumbelliferone by β–galactosidase. Fluorescence was detected using a Hidex (Turku, Finland) CHAME- LEON V plate reader at an excitation wavelength of 315– 395 nm and an emission wavelength of 440–480 nm. Stock solutions of β–galactosidase (52.356 $\mu g\text{-}mL^{-1}$) and MUG (0.591 mM) were prepared in 100 mM sodium phosphate buffer, pH 7.0, containing 1 mM magnesium chloride and 50 mM mercaptoethanol. The stock solutions were further diluted with the buffer solution to obtain assay concentrations of 0.026, 0.052, 0.262, 0.524, 1.047, 2.618, 5.236 and 10.471 $\mu g\text{-}mL^{-1}$ b–galactosidase, and 0.473, 0.236, 0.118, 0.059 and 0.047 mM MUG. Triplicate or quadruplicate kinetic assays were performed separately at 25 °C in 96- well microplates (black Cliniplate; Thermo Fischer Scien- tific, Waltham, MA, USA) by adding 20 μL of substrate solution to 180 μL of enzyme solution. All solutions were thermostatized before use. Fluorescence readings were started approximately 5–6 s after mixing the solutions, and were taken every 2 s throughout the period of constant reaction rate. This period was increasingly shorter as higher enzyme concentrations were investigated: > 16 s for β–galactosidase concentrations lower than 1.047 $\mu g\text{-}mL^{-1}$, approximately 16 s for 2.618 and 5.236 $\mu g\text{-}mL^{-1}$ b–galactosidase, and approximately 8 s for 10.471 $\mu g\text{-}mL^{-1}$ β–galactosidase. Measurements were affected by the inner filter effect, which is noticeable as attenuated fluorescence intensities for higher optical densities. The inner filter effect correction factor that ensures a linear response to the concentration of fluorophore was

determined empirically and then applied to all progress curves.

Egg-white lysozyme enzymatic assay

Time progress curves were measured during hydrolysis of the non-fluorescent substrate MUF-triNAG to the fluorescent product 4−methylumbelliferone by EWL. Fluorescence was detected using a Hidex CHAMELEON V plate reader at an excitation wavelength of 315−395 nm and an emission wavelength of 440−480 nm. Stock solutions of EWL (17.64 μM) and MUF-triNAG (30 μM) were prepared in 50 mM citrate buffer, pH 5.2. The stock solutions were further diluted with the buffer solution in order to obtain assay concentrations of 8.82, 4.41, 2.65, 1.76, 0.88 and 0.18 μM EWL and 15.0, 10.0, 5.0, 2.5, 1.0 and 0.5 μM MUF-triNAG. EWL concentrations were determined by UV absorbance measurements at 280 nm taking into account the presence of 2% contaminants with high molecular-weight estimated by SDS/PAGE analysis. Kinetic assays were performed at 37 °C in 96-well microplates (black Cliniplate; Thermo Scientific) by adding 100 μL substrate solution to 100 μL enzyme solution, and then covering the well with 100 μL paraffin oil to avoid evaporation. All solutions and paraffin oil were thermostatized before use. Fluorescence readings were taken every 30 min throughout the period of constant reaction rate. Lower enzyme concentrations required longer periods for significant product concentration build-up: approximately 2 days for 0.88 μM EWL and approximately 3.6 days for 0.18 μM EWL. Instantaneous product concentrations were deter- mined using a linear calibration curve. No inner filter effect was detectable for the studied range of fluorophore concentrations.

Theoretical calculations

In the present work, a whole picture of single active-site enzyme kinetics without inhibition is given in terms of the influence of the model parameters K_M, v_{max} and K_S, and the model variables time (t), initial enzyme concentration (E_0) and initial substrate concentration (S_0) on the pivotal variable $(S_0 - P)/v$. This picture is more clearly seen using the scaled variables $\tau = K_M/v_{max}$, $e_0 = E_0/K_M$, $s_0 = S_0/K_M$, $\theta = t/(e_0\,\tau)$ and $\beta = (1 - K_S/K_M)$. The following analytical solution is derived in Doc. S1 and used to plot Fig. 1A:

$$\frac{S_0 - P}{v} = \frac{\tau}{2}\left(1 + e_0 + \tilde{s} + \frac{\tilde{\lambda}}{\tanh\left(\frac{\tilde{\lambda}\theta}{2\beta}\right)}\right) \qquad (4a)$$

The definitions of the daughter variables $\tilde{s}, \tilde{\lambda}, s^*$ and θ^* are given by:

$$\tilde{s} = \omega(s^* \exp(s^* - e_0(\theta - \theta^*))) \quad (4b)$$

$$\tilde{\lambda} = \sqrt{(1 + e_0 + \tilde{s})^2 - 4\beta e_0} \quad (4c)$$

$$s^* = \frac{1}{2}\left(s_0 - 1 - e_0 + \sqrt{(s_0 + e_0 + 1)^2 - 4e_0 s_0}\right) \quad (4d)$$

with λ^* corresponding to the value of $\bar{\tilde{\lambda}}$ calculated by Eqn 4c for $\bar{s} = s^*$.

Acknowledgements

The authors gratefully acknowledge receipt of grant numbers SFRH/BPD/73865/2010 (to B.N.E.) and SFRH/BD/74174/2010 (to R.C.) from the Fundação para a Ciência e a Tecnologia, Portugal.

Author contributions

M.F.P., B.N.E., R.C. and P.M.M. performed the experiments and analyzed the data. M.F.P., F.A.R., A.M.D. and P.M.M. conceived and designed the experimental approach. P.M.M. developed the theoretical model. F.A.R., A.M.D. and P.M.M. wrote the manuscript.

References

1. Johnson KA & Goody RS (2011) The original Michaelis constant: translation of the 1913 Michaelis- Menten paper. *Biochemistry* 50, 8264–8269.
2. Michaelis L & Menten ML (1913) Die Kinetik der Invertinwirkung. *Biochem Z* 49, 333–369.
3. Bobkova EV, Weber MJ, Xu Z, Zhang Y-L, Jung J, Blume-Jensen P, Northrup A, Kunapuli P, Andersen JN & Kariv I (2010) Discovery of PDK1 kinase inhibitors with a novel mechanism of action by ultrahigh throughput screening. *J Biol Chem* 285, 18838–18846.
4. Wienkers LC & Heath TG (2005) Predicting *in vivo* drug interactions from *in vitro* drug discovery data. *Nat Rev Drug Discovery* 4, 825–833.
5. Gunawardena J (2012) Some lessons about models from Michaelis and Menten. *Mol Biol Cell* 23, 517.
6. Davidson EA, Samanta S, Caramori SS & Savage K (2012) The dual Arrhenius and Michaelis-Menten kinetics model for decomposition of soil organic matter at hourly to seasonal time scales. *Glob Change Biol* 18, 371-384
7. Gunawardena J (2014) Time-scale separation - Michaelis and Menten's old idea, still bearing fruit. *FEBS J* 281, 473–488.
8. Cornish-Bowden A (2013) The origins of enzyme kinetics. *FEBS Lett* 587, 2725–2730.

9. English BP, Min W, van Oijen AM, Lee KT, Luo G, Sun H, Cherayil BJ, Kou S & Xie XS (2005) Ever- fluctuating single enzyme molecules: Michaelis-Menten equation revisited. *Nat Chem Biol* 2, 87-94.
10. Xie XS (2013) Enzyme kinetics, past and present. *Science* 342, 1457−1459.
11. Deichmann U, Schuster S, Mazat JP & Cornish- Bowden A (2014) Commemorating the 1913 Michaelis− Menten paper Die Kinetik der Invertinwirkung: three perspectives. *FEBS J* 281, 435−463.
12. Briggs GE & Haldane JBS (1925) A note on the kinetics of enzyme action. *Biochem J* 19, 338−339.
13. Segel LA (1988) On the validity of the steady state assumption of enzyme kinetics. *Bull Math Biol* 50, 579−593.
14. Berberan-Santos MN (2010) A general treatment of Henri−Michaelis−Menten enzyme kinetics: exact series solution and approximate analytical solutions. *MATCH Commun Math Comput Chem* 63, 283−318.
15. Hanson SM & Schnell S (2008) Reactant stationary approximation in enzyme kinetics. *J Phys Chem A* 112, 8654−8658.
16. Cao W & De La Cruz EM (2013) Quantitative full time course analysis of nonlinear enzyme cycling kinetics. *Sci Rep* 3.
17. Bajzer Ž & Strehler EE (2012) About and beyond the Henri−Michaelis−Menten rate equation for single- substrate enzyme kinetics. *Biochem Biophys Res Commun* 417, 982−985.
18. Chen WW, Niepel M & Sorger PK (2010) Classic and contemporary approaches to modeling biochemical reactions. *Genes Dev* 24, 1861−1875.
19. Rami Tzafriri A & Edelman ER (2007) Quasi-steady- state kinetics at enzyme and substrate concentrations in excess of the Michaelis-Menten constant. *J Theor Biol* 245, 737−748.
20. Schnell S & Maini P (2000) Enzyme kinetics at high enzyme concentration. *Bull Math Biol* 62, 483−499.
21. Houston JB & Kenworthy KE (2000) *In vitro−in vivo* scaling of CYP kinetic data not consistent with the classical Michaelis-Menten model. *Drug Metab Dispos* 28, 246−254.
22. Cornish-Bowden A (2012) Fundamentals of Enzyme Kinetics, 4th edn. Wiley, Weinheim.
23. Fersht AR & Jakes R (1975) Demonstration of two reaction pathways for the aminoacylation of tRNA. Application of the pulsed quenched flow technique. *Biochemistry* 14, 3350−3356.
24. Duggleby RG (2001) Quantitative analysis of the time courses of enzyme-catalyzed reactions. *Methods* 24, 168−174.
25. Crespo R, Rocha FA, Damas AM & Martins PM (2012) A generic crystallization-like model that describes the kinetics of amyloid fibril formation. *J Biol Chem* 287, 30585−30594.
26. Tipton KF, Armstrong RN, Bakker BM, Bairoch A, Cornish-Bowden A, Halling PJ, Hofmeyr J-H, Leyh TS, Kettner C, Raushel FM *et al.* (2014) Standards for reporting enzyme data: the STRENDA Consortium. What it aims to do and why it should be helpful. *Perspect Sci* 1, 131−137.

27. Xu Y, Strickland EC & Fitzgerald MC (2014) Thermodynamic Analysis of Protein Folding and Stability Using a Tryptophan Modification Protocol. *Anal Chem* 86, 7041–7048.
28. Bennett BD, Kimball EH, Gao M, Osterhout R, Van Dien SJ & Rabinowitz JD (2009) Absolute metabolite concentrations and implied enzyme active site occupancy in *Escherichia coli*. *Nat Chem Biol* 5, 593–599.
29. Reuveni S, Urbakh M & Klafter J (2014) Role of substrate unbinding in Michaelis-Menten enzymatic reactions. *Proc Natl Acad Sci USA* 111, 4391–4396.
30. Fendt SM, Buescher JM, Rudroff F, Picotti P, Zamboni N & Sauer U (2010) Tradeoff between enzyme and metabolite efficiency maintains metabolic homeostasis upon perturbations in enzyme capacity. *Mol Syst Biol* 6, 1.
31. Blume A, Angulo J, Biet T, Peters H, Benie AJ, Palcic M & Peters T (2006) Fragment-based screening of the donor substrate specificity of human blood group B galactosyltransferase using saturation transfer difference NMR. *J Biol Chem* 281, 32728–32740.
32. Sergienko EA & Mill an JL (2010) High-throughput screening of tissue-nonspecific alkaline phosphatase for identification of effectors with diverse modes of action. *Nat Protoc* 5, 1431–1439.
33. Copeland RA (2005) Evaluation of Enzyme Inhibitors in Drug Discovery: A Guide for Medicinal Chemists and Pharmacologists. Wiley, New-York.

Supporting information

Additional supporting information may be found in the online version of this article at the publisher's web site:

Fig. S1. Validation of the theoretical model.

Fig. S2. Worst-case correlation between numeric and theoretical solutions.

Fig. S3. Deviations from the hyperbolic and linear relationships under MM conditions.

Fig. S4. Early reaction phases are K_S/K_M-sensitive for high e_0.

Fig. S5. Later reaction phases are K_S/K_M-sensitive for e_0 of approximately 1.

Fig. S6. Time needed to reach the stationary point. Fig. S7. Model predictions in a different perspective. Fig. S8. Early reaction phases are sensitive to small variations of K_S/K_M for $e_0 > 1$.

Doc. S1. Derivation of equations presented in the text.

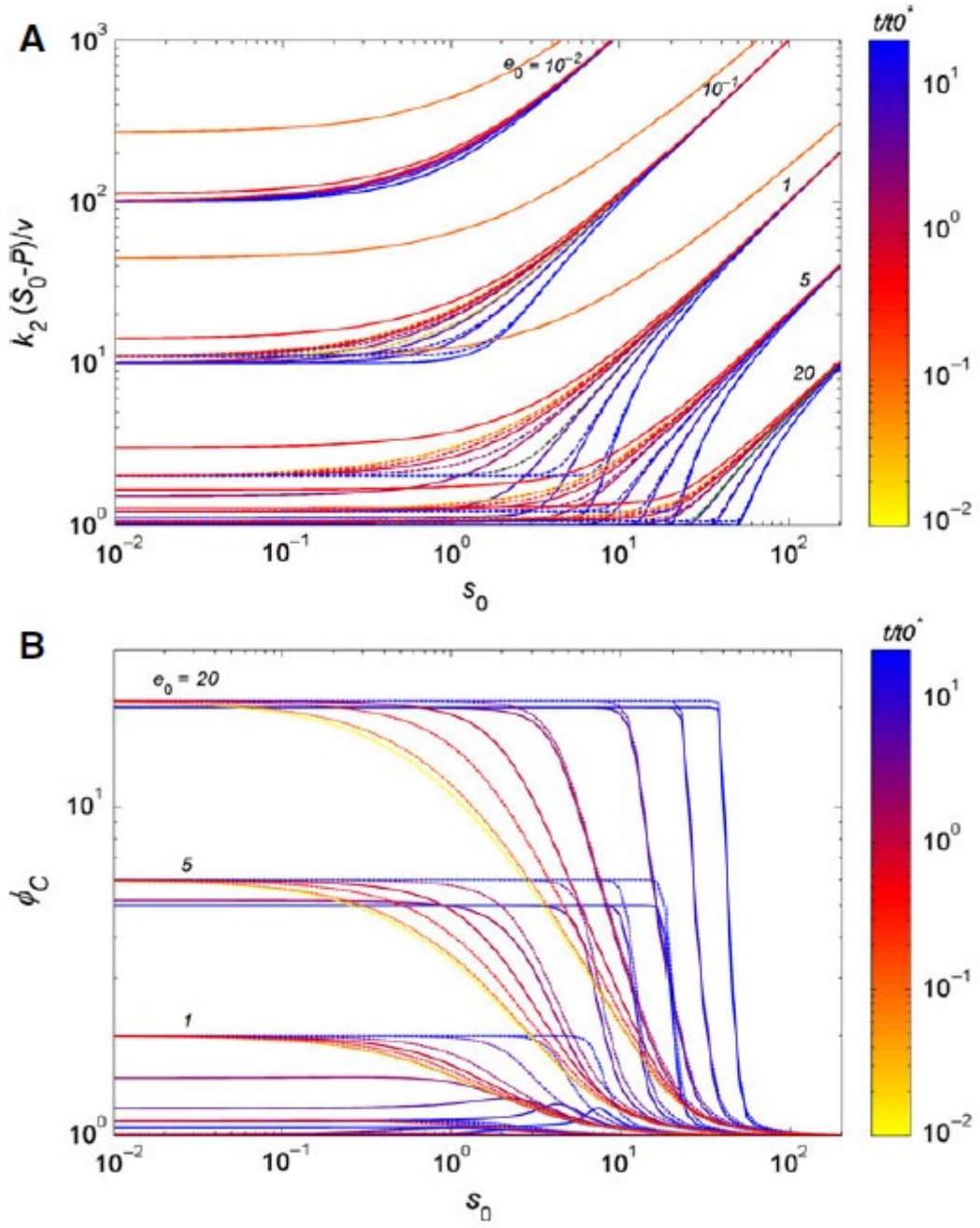

Fig. 1. The complete picture of single active-site enzyme kinetics without inhibition. Log–log plots of model Eqn 2: (A) in its extended form (equivalent to Eqn 4), and (B) focusing on the definition of correction factor ΦC (Eqn S23, Doc. S1). The influence of the *K*M-normalized initial concentration of substrate (*s*0) on (A) the *k*2 pivotal variable product *k*2 (*S*0 – *P*)/*v*, and (B) the correction factor ΦC is shown for limiting values of *K*S/*K*M = 0 (solid lines) and *K*S/*K*M = 1 (dashed lines). Italic numbers indicate characteristic values of the *K*M-normalized initial concentration of free enzyme (*e*0) used to calculate the series of curves. The gradation of colors represents the time progression of the enzymatic reaction relative to the stationary instant *t*0* calculated for *K*S/*K*M = 0 using Eqn S17 (Doc. S1). Earlier reaction phases are not represented for *K*S/ *K*M = 0 to avoid superposition of curves calculated for different *e*0 values. Figs S4, S7 and S8 provide a more detailed analysis of earlier reaction phases. In addition, ΦC curves calculated for $e0 \leq 10^{-1}$ are not shown in (B) as their values do not differ considerably from 1. Figs S1 and S2 show the validation of the model against the exact numeric solution.

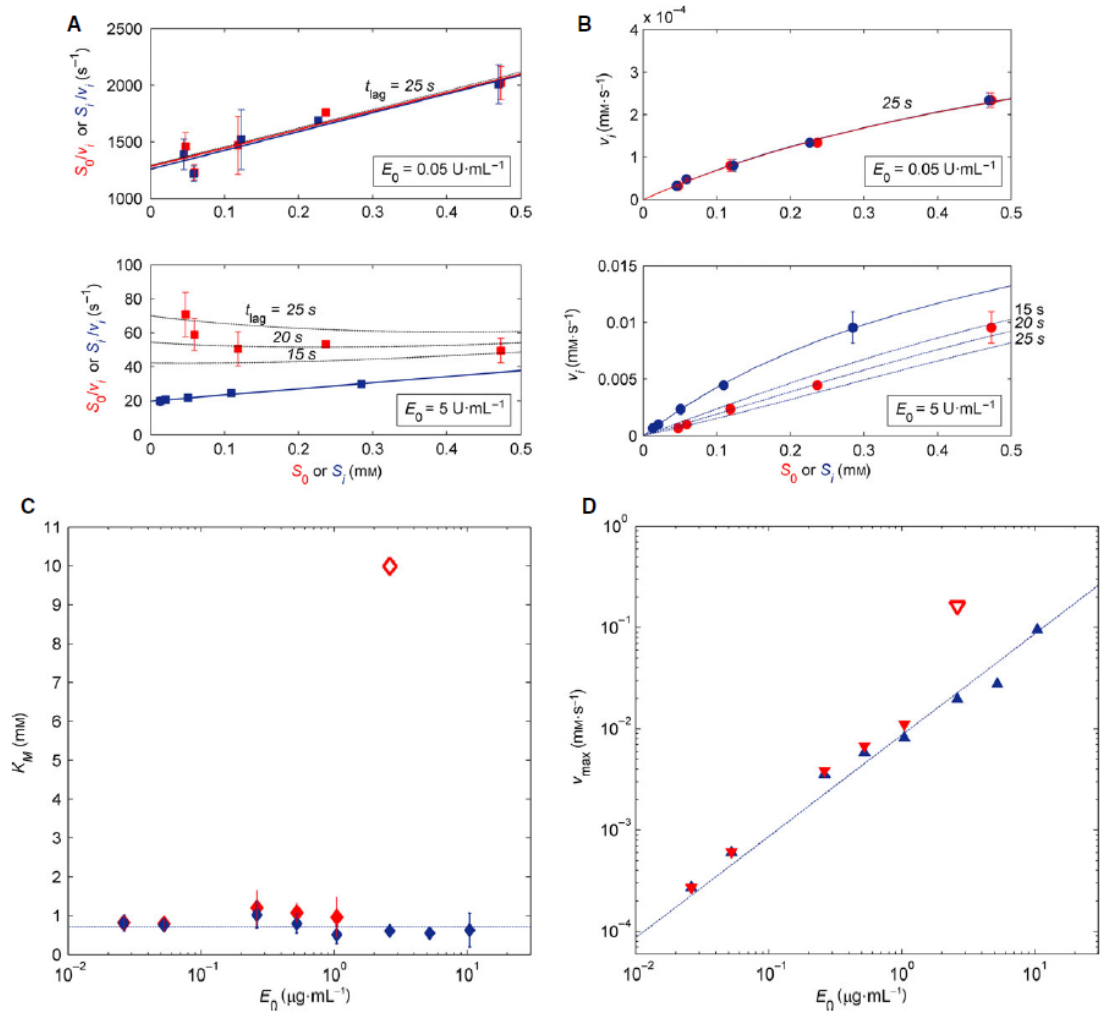

Fig. 2. Estimating *v*max and *K*M parameters under MM conditions. Illustrative example for hydrolysis of MUG substrate by the enzyme β-galactosidase at 25 °C and pH 7.0. The typical method (red) analyses the effect of true initial concentrations of substrate (*S*0) on the initial

reaction rate (vi), while the modified method (blue) analyses the effect of measured initial concentrations of substrate (Si) on vi. Differences between true concentrations (subscript 0) and measured concentrations (subscript i) arise from the time lag ($t$lag) preceding each measurement. The typical method did not provide reliable estimations of the kinetic constants for $E0 > 2.618$ μg-mL^{-1}. (A) Examples of Hanes–Woolf plots for initial concentrations of free enzyme $E0 = 0.052$ μg-mL^{-1} (top) and 5.236 μg-mL^{-1} (bottom). Symbols and error bars are means ± standard deviations of triplicate or quadruplicate measurements. Solid lines represent valid linear fits. Dotted lines represent theoretical $S0/v$i versus $S0$ plots predicted by Eqn 2 under MM conditions ($\Phi C = 1$) for the lag time indicated by italic numbers, and using $v$max and KM parameters obtained by the modified method. (B) Same data as in (A) represented as vi versus substrate concentration plots. (C) Fitted KM parameters (closed symbols) represented on semi-log scale as a function of $E0$. The dotted blue line represents mean KM values. Error bars represent 95% confidence intervals. (D) Fitted $v$max parameters (closed symbols) represented on a log–log scale as a function of $E0$. The dotted blue line represents the linear fit with intercept set to 0. Open red symbols in (C) and (D) are examples of invalid results (for which the 95% confidence intervals include 0).

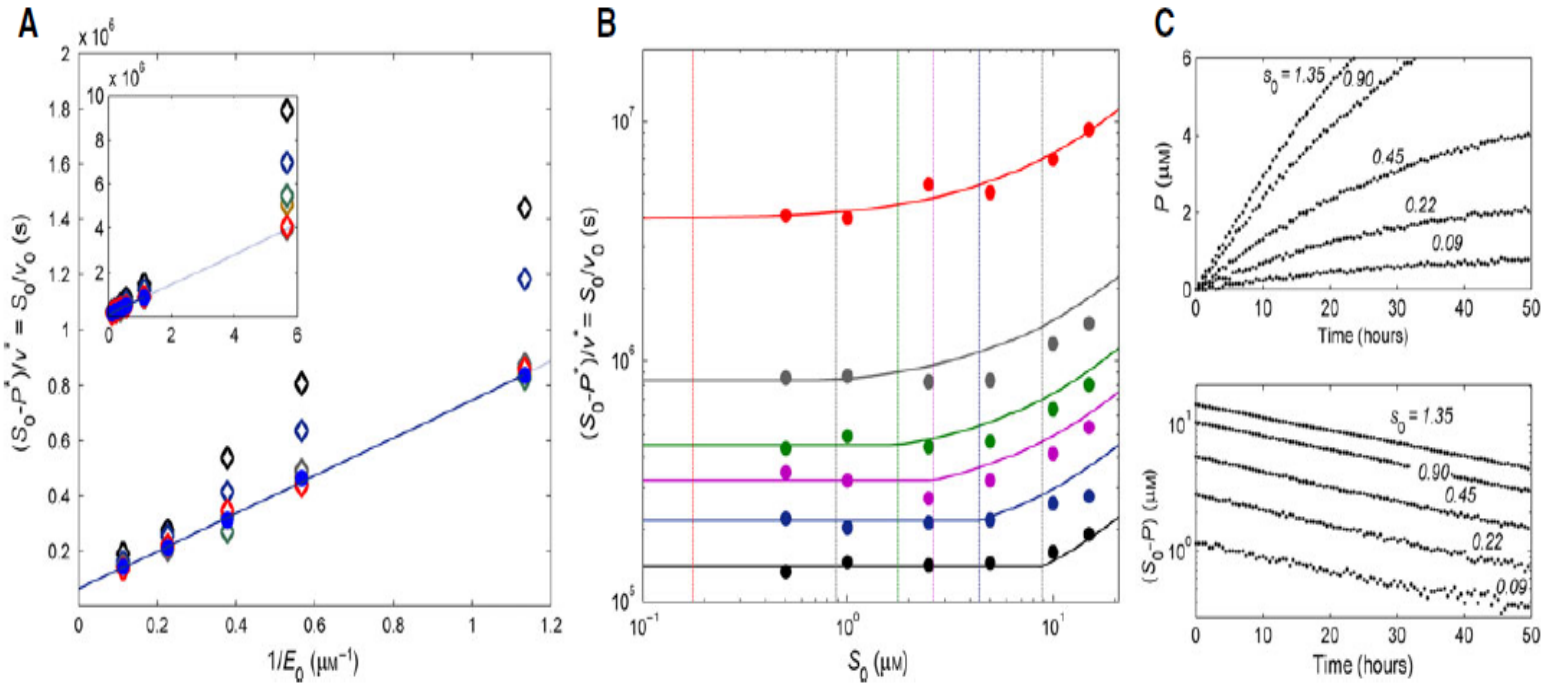

Fig. 3. Estimating *k*2, *K*M and *K*S parameters under non-MM conditions. Illustrative example for hydrolysis of MUF-triNAG substrate by hen egg-white lysozyme at 37 °C and pH 5.2. (A) Open diamonds represent the measured stationary pivotal variable ($S0 - P^*)/v^*$ as a function of the reciprocal of the free enzyme concentration $E0^{-1}$ for $S0$ = 15.0 μM (black diamond), 10.0 μM (blue diamond), 5.0 μM (brown diamond), 2.5 μM (green diamond), 1.0 μM (gray diamond) and 0.5 μM (red diamond). Closed circles represent mean $(S0 - P^*)/v^*$ values measured under $S0 < E0$ conditions for each enzyme concentration. The solid blue line represents the linear fit of Eqn 3 to the data represented by the closed symbols. Fitting results: $k2 = vmax/E0 = 16.1 \pm 2.0 \times 10^{-6}$ s^{-1}; $KM = 11.1 \pm 1.5$ μM. Inset: use of an expanded axis for regions of $E^{-1} > 0.88^{-1}$ μM^{-1}. The light blue line represents the linear fit extrapolated to $S0 > E0$ conditions. (B) Closed circles represent measured $(S0 - P^*)/v^*$ values as a function of $S0$ for $E0$ = 8.82 μM (black circle), 4.41 μM (blue circle), 2.65 μM (purple circle), 1.76 μM (green circle), 0.88 μM (gray circle) and 0.18 μM (red circle). A log–log plot is used

for clarity. Solid lines represent theoretically predicted curves using Eqn 3 and the fitted parameters determined in (A). Vertical dotted lines represent boundaries at $S0 = E0$. (C) Examples of progress curves measured at $E0$ = 8.82 μM (s = 21.7 h) under *K*S-sensitive conditions, i.e. for values of $e0$ (0.79) and $s0$ (italic numbers) close to or < 1. Top panel: product accumulation curves showing no inflection points ($v^* = v0$ and $P^* = 0$) independently of the value of $S0$. Bottom panel: concentration of product still to be formed ($S0 - P$) represented in a log–linear plot as a function of time; instantaneous slopes correspond to the reciprocal of the pivotal variable $v/(S0 - P)$. The hyperbolic trend (top panel) and linear trend (bottom panel) are indicators that *K*S = *K*M (11.1 μM).